# Development of an optimal gas diffusion medium for polymer electrolyte membrane fuel cells and assessment of its degradation mechanisms

*Saverio Latorrata*[*], *Paola Gallo Stampino*, *Cinzia Cristiani*, *Giovanni Dotelli*

*Department of Chemistry, Materials and Chemical Engineering "Giulio Natta", Politecnico di Milano, piazza Leonardo da Vinci 32, 20133 Milan, Italy*

Received 23 February 2015
Received in revised form
10 May 2015
Accepted 14 May 2015
Available online 6 June 2015

## Introduction

Fuel cells are considered as one of the most important and promising devices for green-energy production for both portable and non-portable systems. Among the wide variety of available technologies, polymer electrolyte membrane fuel cells (PEMFCs) have been largely investigated by research groups worldwide, leading to a continuous optimization of each component of the device [1–4].

In order to make fuel cells competitive with internal combustion engines, among others, the durability is a key point to be assessed. In this respect, automotive fuel cell power systems need to reach an operating lifetime of 5000 h (approximately 7 months at the vehicle operating conditions, including variable relative humidity, shutdown/start-up, freeze/thaw, and subfreezing down to −40 °C), whereas, for stationary fuel cells an operating lifetime of more than 40,000 h (approximately 4.5 years of continuous operation) is required [5]. However, currently, such targets have not been

* *Corresponding author*. Tel.: +39 02 23993233; fax: +39 02 23993280.
E-mail address: saverio.latorrata@polimi.it (S. Latorrata).

achieved yet. Thus, an intensive research is still needed to address the issues related to PEMFCs durability or degradation in order to achieve a competitive commercialization. Degradation in PEMFCs occurs mainly with mechanical or chemical mechanisms, leading to a loss of performance of the device over time. These phenomena have been widely investigated and can affect each component of the fuel cell, from the external bipolar plates to the inner polymeric electrolytic membrane [5–8].

Several research groups have developed accelerated stress tests (ASTs) in order to evaluate the electrical behavior of laboratory scale products in long-time activities without testing the samples for thousands of hours [5,9–24]. Such tests are usually based on a combination of different stress parameters, such as potential control, undesirable temperatures, humidity or load cycling, and on measurements of the consequent both electrical and morphological response. Other works proved a direct connection of changes in microstructure and in surface characteristics of gas diffusion media (GDM) with global electrochemical performance and water transport properties [6,8,14,16,21,24–30].

The gas diffusion layer (GDL) and the micro-porous layer (MPL) are crucial components in the PEMFC assembly [2,31,32]. They are, respectively, a macro-porous carbon cloth substrate based on carbon fibers and a thin layer coated onto the former and made of carbon nano-particles mixed with a hydrophobic polymeric agent. It has been demonstrated that their use leads to a considerable improvement of global performance of de-vices, allowing to enhance reactants and water transport, electronic and thermal conduction and providing mechanical support to the membrane-electrode assembly [2,33,34]. However, at the state of the art, there is no established standard protocol dealing with the durability testing of these components [5,9].

Therefore, the development of a fast standardized and analytic method to experimentally evaluate the degradation phenomena of the components, both at the lab- and production-scale, would be desirable. As mentioned, some studies about the GDL/MPL (i.e. the GDM, gas diffusion media) degradation already available in the literature demonstrated a loss of hydrophobicity and changes in porosity when they are processed with an acidic solution at medium-temperature [35]; both GDM modifications result in an increase of the retained water content thus impeding gas phase mass transport [36,37]. However, it should be noted that the carbon fibers of the GDL and the carbon black particles of the MPL are more stable than the carbon black in the catalyst layer due to the absence of Pt which can catalyze the electrochemical oxidation of carbon and its consequent degradation [5]. In situ, stress effects, which have been used to assess GDM stability, include freezing/de-freezing cycles and fuel starvation. For instance, Kim et al. [38] reported interfacial delamination between the catalyst layer and GDM after 100 freezing/de-freezing cycles from −40 °C to 70 °C, which resulted in ice formation and significantly increased GDM deformation. Oszcipok et al. [39] observed a decrease of the GDM surface hydrophobicity in cold-start conditions. Other studies examined GDM degradation using ex-situ methods, which may be helpful in order to separate GDM response from that one of other components. Such stress parameters try to simulate the complex environment during fuel cell operation [26,27,29]; for instance, GDLs can be submerged in hydrogen peroxide solution, a method similar to Fenton's test, and in this way weight losses and changes in the MPL contact angle may be detected [40]. Other authors soaked GDL samples in liquid water at different oxygen concentrations and correlated the decrease in hydrophobicity with exposure time and water temperature [41]. Finally, Chun et al. [6] designed an innovative dummy cell without any catalyst layer and developed an accelerated stress test to investigate the progress of the MPLs mechanical degradation during a short period of time.

In this work, details about the development of ex-situ accelerated stress tests, both chemical and mechanical, on optimized samples to study GDMs durability are given. Indeed, carbon nanotubes (CNTs), partially replacing carbon black in the MPL ink formulation, were added in order to achieve a better conductivity of the final sample and, as hydrophobic agent, FEP was employed, being able to reduce diffusive limitations during the running of the fuel cell better than the traditionally employed PTFE, as demonstrated in a previous work by the authors [42]. Even though much less conventional than PTFE as a hydrophobic agent, FEP was already employed by other research groups to make GDMs for PEM fuel cells hydrophobic [43–49]. Some of them also employed carbon nanotubes in order to get better performance [48]. Moreover, CNTs were found to be more corrosion-resistant than carbon black [20].

In this work, authors tried to achieve a compromise between GDM composition, preparation route and durability. Changes in properties of the prepared samples were checked by periodic analyses to evaluate if any modification occurred on hydrophobicity, material loadings, morphology and electrochemical performance.

A procedure to investigate chemical and mechanical resistance of the optimized GDMs was developed, with a particular attention to get information on degradation mechanisms and on the role of GDMs components.

## Experimental

### *Preparation*

On the basis of a previous work [50], carbon nanotubes (CNTs, Nanothinx NTX1, purity: 97%, diameter: 10–30 nm, length: 10 μm, metal particles: 3 wt %), partially replacing carbon black powder, were used in order to make final coatings more conductive than the standard one. Moreover, inks containing a hydrophobic agent other than PTFE (i.e. FEP, fluorinated ethylene propylene), already proven to be superior [42], were experienced to evaluate the effect of coupling both the increased conductivity and the enhanced hydrophobicity. Thus, on the basis of the preparation described in Ref. [42], a slurry was formulated mixing a FEP-containing dispersion supplied by DuPont (55% wt), and isopropyl alcohol (IPA, Sigma Aldrich) in deionized water; then, carbon black (CB, Vulcan XC72R from Cabot) and CNTs were slowly added. The mixture was vigorously stirred and homogenized by a high shear mixer (UltraTurrax T25) at 8000 rpm for 10 min. The following composition was selected: $(CB + CNTs)/H_2O = 0.13$

(w/w), FEP/(CB + CNTs) = 0.12 (w/w) and (CB + CNTs)/IPA = 5.6 (w/w). Three different CNTs/CB ratios were experienced, 10%, 5% and 1% wt, in order to investigate the effect of CNTs content on physical and electrochemical properties of the final GDMs. The so-obtained inks were deposited onto FEP pretreated GDL substrates via the blade coating technique (velocity of 15.4 mm/s, gap of 40 μm, shear rate of about 350 $s^{-1}$) to form the micro-porous layers [42]. Finally, the samples were calcined up to 260 °C to remove water, IPA and to sinter FEP, as reported in Ref. [42].

### *Characterization*

Rheology measurements were performed on the inks in order to verify their suitability for blade coating deposition. The rheological behavior of the inks was tested at 20 °C by means of a rotational rheometer (Rheometrics DFR 200). A 40 mm parallel-plates geometry was employed and a 1 mm gap between the stationary plate and the movable one was set. Dynamic viscosities were investigated in the shear rate range $10^{-3}$–$10^{3}$ $s^{-1}$.

Static contact angle measurements, SEM analyses and mercury intrusion porosimetry were used to assess GDMs morphology; finally, polarization curves and EIS allowed to evaluate the influence of such GDMs on overall fuel cell performances.

The samples hydrophobicity was assessed by static contact angles measurements according to the sessile drop technique using an OCA 20 Dataphysics instrument. Values reported for each sample are the result of the average of ten measurements [51].

Scanning electron microscope (Cambridge Stereoscan 360) was used for the morphological analyses of both surface and cross-section of the GDMs. Samples were previously gold coated to prevent charging effects.

Porosity and pore size distribution of the GDMs were measured by the mercury intrusion technique using a Carlo Erba Porosimeter 2000 Series instrument. The pore size distributions were calculated by applying the Washburn equation.

Electrical and electrochemical tests were carried out at two temperatures (60 °C and 80 °C) and two relative humidity conditions (80–100% and 80–60%, anode–cathode). Flow rates were 0.2 and 1.0 NL/min for hydrogen and air, respectively. A commercial catalyst coated membrane (CCM, supplied by Baltic Fuel Cells), which consists of catalyst layers (active area of 23 $cm^2$) directly coated onto a 50 μm thick Nafion membrane, was employed as MEA. Platinum loading was 0.3 and 0.6 mg/$cm^2$ at the anode and the cathode, respectively.

Polarization curves were recorded under galvanostatic conditions in the current density range from OCV to 1.32 A/$cm^2$, with steps of 0.09 A/$cm^2$. In the same range, electrochemical impedance spectroscopy (EIS) was carried out by using a frequency response analyzer (FRA, Solartron 1260). All impedance spectra were obtained over a frequency range of 0.5 Hz–1 kHz (10 points per decade). Five spectra per each current density value were acquired and each impedance spectrum finally used in the discussion was the result of an averaging procedure. The typical spectrum of a running fuel cell is composed by one, two or, more rarely, three arcs, whose origin can be attributed to two well distinguished physical phenomena: activation polarization and mass transfer limitations. All the experimental data were fitted using the Zview® software (Scribner Associates) by using the equivalent circuit shown in Fig. 1 in order to determine the different contributions to voltage losses [52].

At low current density, the equivalent circuit used (Fig. 1a) is made of a resistance ($R_s$) in series with two parallel resistance/constant phase element circuits, $R_{p,a}$/$CPE_{,a}$ and $R_{p,c}$/$CPE_{,c}$. $R_s$ represents the ohmic losses, while the first circuit ($R_{p,a}$/$CPE_{,a}$) models the anodic activation polarization (i.e. charge transfer resistance at the anodic catalyst) when visible and the second one ($R_{p,c}$/$CPE_{,c}$) the activation losses related to the cathode, which are always observable and more pronounced than anodic ones, because of the sluggish kinetics of the oxygen reduction. Obviously, when it is not possible to identify anodic activation losses the first parallel circuit of Fig. 1 disappears. At medium and high current density, another element is necessary to model the flooding phe-nomena at lower frequency (i.e. mass transfer limitations). Thus, the parallel circuit $R_d$/$CPE_d$ is added in series with cathodic activation polarization resistance (Fig. 1b).

Constant phase elements (CPE) were used instead of pure capacitances, to account for the capacitive losses which generally occur in porous electrodes; in fact, the phase of CPE parameters did not dramatically deviate from unity (0.85–1.00) [30,53].

Evaluation of durability was also performed by keeping the fuel cell at constant current density (0.5 A/$cm^2$) for 1000 h,

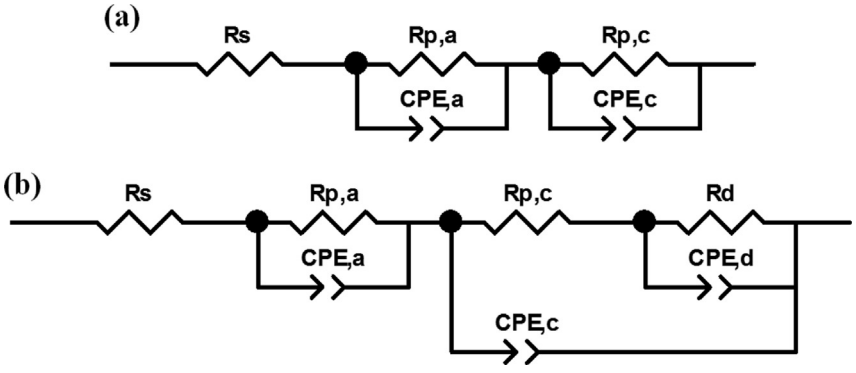


**Fig. 1 – Equivalent circuits used for fitting EIS data at low current densities (<0.4 A/$cm^2$) (a) and at high current densities (>0.4 A/$cm^2$) (b).**

monitoring both voltage and cell efficiency trends as a function of time.

### *Accelerated stress tests*

Both chemical and mechanical degradation can occur in GDMs during fuel cell operations. Chemical degradation can be generated by carbon corrosion and/or polymer decomposition [8], while mechanical degradation, mainly due to gases flow in presence of water, is related to detachment of material, in particular carbon layers of the MPL.

Thus, two different separated ex-situ experiments were designed to analyze the effect and the mechanism of each degradation phenomenon. The chemical AST was performed by soaking GDMs in a 20% v/v sulfuric acid solution at pH equal to 0, far below the typical pH value (2–3) of the running cell environment, for a total time of 1000 h. This harsher condition would accelerate the chemical degradation of GDMs. Changes in physical-chemical and morphological properties of the samples were assessed at intermediate ageing times (168 h, 336 h, 504 h, 672 h, 840 h, 1000 h) over the whole test period; in addition to that, the performance of fuel cells assembled with aged GDMs was tested too.

The mechanical AST was carried out on the basis of a recent literature study [6], but a simpler system was developed. A dummy cell was created consisting of two GDMs both at the anodic and cathodic side, separated by a 50 μm Nafion 212 plain membrane, i.e. without any catalyst, in order to avoid any possible electrochemical stress and degradation. Only air was fed on either side at a flow rate of 2 NL/min, considerably higher than those employed during standard running (0.2 and 1.0 NL/min for hydrogen and air, respectively) for accelerating me-chanical degradation. This air stream was fully humidified (RH: 100%). This operating condition, together with the high inlet flow value, should favor fast degradation. In the case of the mechanical AST, GDMs properties were evaluated only at the end of the ageing treatment, i.e. 1000 h.

Operating conditions after ASTs were set at 60 °C and RH (A-C) 80–100%, where the best performances were obtained in standard conditions.

## Results and discussion

### *Rheological characterization*

In Fig. 2 the flow curves of the inks containing the different CNTs concentrations are compared with that of a corresponding CNTs-free ink, developed in Ref. [42].

All the samples are pseudo-plastic, therefore suitable for blade coating deposition [54], showing a viscosity which decreases upon increasing the shear rate.

All the four curves are very close, practically overlapped, over the whole investigated shear rate range.

### *Static contact angle measurements*

The average static contact angles measured at room temperature on GDMs surface upon thermal treatment are reported in Table 1.

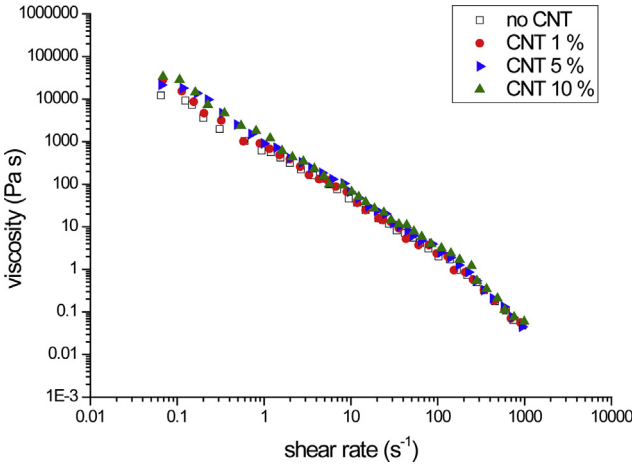


**Fig. 2 – Flow curves of inks containing and non-containing CNTs.**

**Table 1 – Average contact angle (ten measurements) of the samples with different CNTs content (by weight).**

| Sample | Contact angle (°) |
|---|---|
| No CNT | 159.5 ± 2.1 |
| CNT 1% | 160.7 ± 2.8 |
| CNT 5% | 159.3 ± 2.8 |
| CNT 10% | 158.5 ± 2.1 |

Contact angles higher than 150° were measured, thus the superhydrophobicity range was achieved for all the samples. No sensible variation of the contact angles is observed among the samples as values around 160° are always detected, thus suggesting that no effect of the CNTs concentration on hydrophobicity can be inferred, which in turn can only be ascribed to nature and concentration of the hydrophobic polymer, i.e. FEP. It has to be underlined, indeed, that the considered GDMs were formulated to contain the same FEP content, therefore very close, though not equal, contact angle values were measured. It can be worth to note that the contact angle of conventional PTFE-based GDM does not exceed 150° [42].

### *Mercury intrusion porosimetry*

The pores size distribution of the three GDMs containing CNTs was measured and compared (Fig. 3) with that one of the FEP-based GDM without CNTs, aiming to evaluate possible effects of the CNTs concentration on final porosity.

Meso-pores are not present and macro-porosity, due to cracks generated during thermal treatment, exhibited a polymodal distribution.

The samples showed similar micro-pores dimensions, all in the range 0.044–0.049 μm, and similar volumes, 0.22–0.24 cc/g, even though the GDM containing 10% wt CNTs showed a slightly higher value (0.31 cc/g) with respect to the others. However, a specific effect of the CNTs concentration cannot be found.

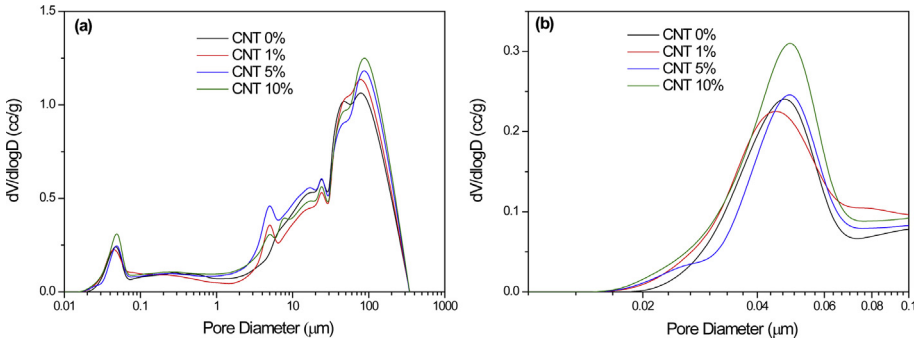


**Fig. 3 – Pores size distribution for FEP-based GDMs with different concentrations of CNTs (a) and off-set of the micro-porous region (b).**

*Electrochemical characterization*

Polarization and power density curves obtained for fuel cells assembled with GDMs containing different amounts of CNTs are shown in Fig. 4 and compared with those obtained for a CNT-free sample with the same amount of FEP.

As expected, electrical properties and performances are influenced by CNTs amount. Indeed, from Fig. 4, it is clear that the best performances, at any operating condition, were found for the highest CNTs amount. At 60 °C and high cathodic RH (Fig. 4a), the GDM containing the maximum amount of CNTs (10% wt) was able to guarantee the highest power density value, 0.7 W/cm$^2$. In addition to that, the same sample always showed, in the medium current density region, the lowest slopes of the polarization curves, which implies the lowest ohmic resistances. These behaviors are clearly due to the

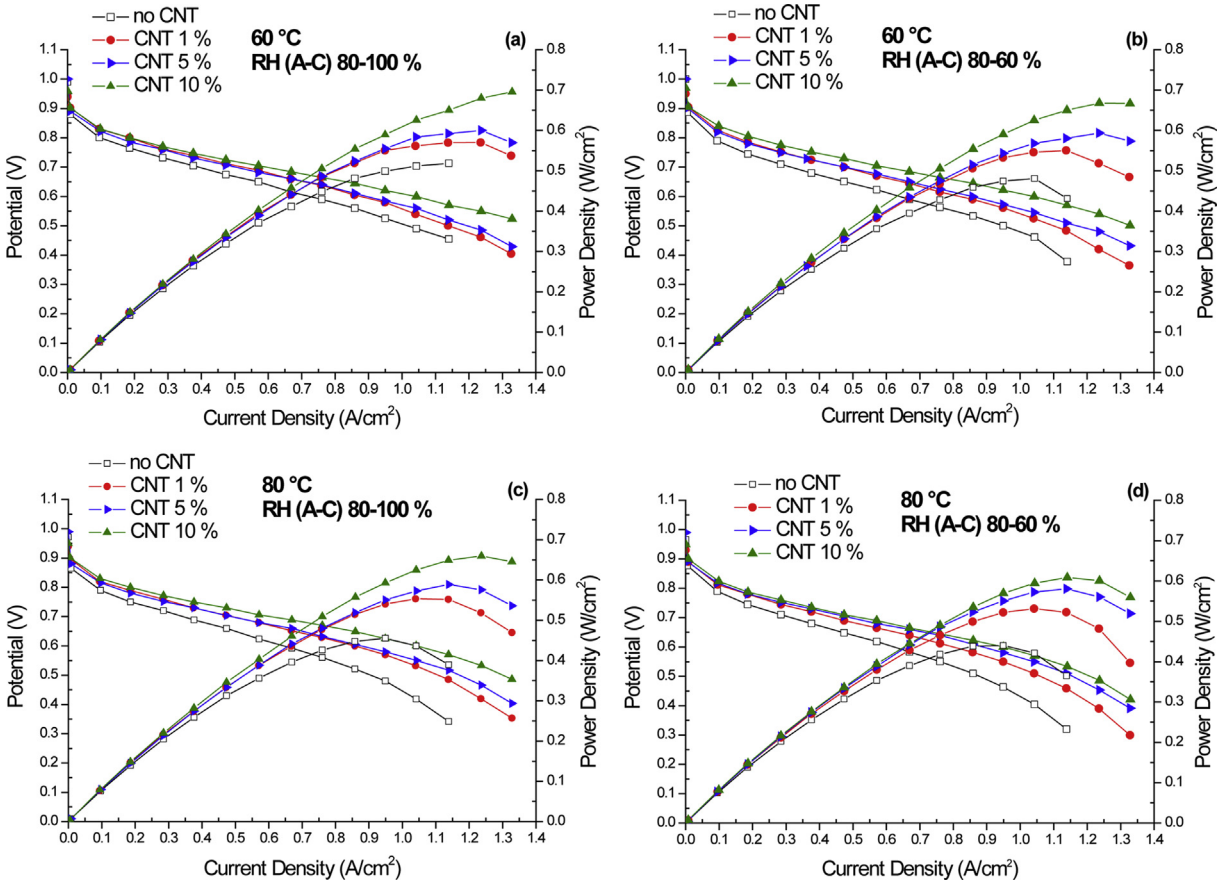


**Fig. 4 – Polarization and power density curves obtained for fuel cells assembled with FEP-based GDMs with different CNTs content. Operating conditions: a) 60 °C, RH (A-C): 80–100%; b) 60 °C, RH (A-C): 80-60%; c) 80 °C, RH (A-C): 80–100%; d) 80 °C, RH (A-C): 80-60%.**

considerably higher conductivity of CNTs with respect to conventional carbon black powder. Thus, the higher the CNTs content the better the electrical performances. However, for this work, no further increase above 10% wt of the CNTs content was considered acceptable from an economical point of view since CNTs, it is well known, are very expensive. Moreover, CNTs are effective to reduce the concentration overpotential as pointed out by the less pronounced slope of polarization curves of CNTs-based samples at the high current density region. This might be due to surface arrangement of nanotubes in the MPL. Indeed, their ordered and elongated structure is likely able to guarantee a better and more efficient molecular diffusion than carbon black one, which on the contrary can make molecules path more tortuous. Particularly at high current density, when more water is generated, CNTs behavior can be more effective and facilitate the management of water, thus reducing mass transfer limitations and conse-quently concentration overpotential.

After conventional electrical tests, fuel cells assembled with FEP-CNT-based GDMs were run at constant current density (0.5 A/cm$^2$) for 1000 h in order to test their durability; the voltage degradation rate (μV/h) and the evolution of the cell efficiency over the time were considered significant parameters for the system evaluation. Only one operating condition was employed, namely 60 °C and RH 80–100%, i.e. at which the best performance in terms of output power and polarization was achieved (see Fig. 4).

Fuel cell efficiency is defined as the ratio between the electricity produced and the consumed hydrogen [1,5]:

$$\eta = W_{el}/W_{Hydr} = V \cdot I/(HHV \cdot I/nF) \cdot \eta fu = V \cdot \eta fu/1.482$$

where HHV is the hydrogen higher heating value (286 kJ/mol) and $\eta_{fu}$ is the "fuel utilization" which takes into account hydrogen losses and it is the reciprocal of stoichiometric ratio (actual hydrogen flow rate over theoretically calculated hydrogen flow rate).

The efficiencies of the cells with the three different GDMs containing CNTs (Fig. 5), calculated after monitoring the voltage, are quite constant over time. This suggests that if a fuel cell generates energy in the ohmic region (i.e. medium current density), as it is in the practice, the system should exhibit constant performance over time. Indeed, restrained degradation rates were obtained: 14, 15 and 32 μV/h for GDMs with 10, 5 and 1% wt of CNTs, respectively; it is worth noting that degradation rate of a commercial system (from Baltic Fuel Cells) at the same operating condition is 30 μV/h, thus suggesting a pretty durability of the materials used in our cell assembly, despite not optimized for commercialization. As expected, the GDM containing the highest value of CNTs showed the best fuel cell mean efficiency (more than 40%); however, the efficiencies obtained with the other two samples are also satisfying, being only slightly lower than 40%.

A further confirmation of the good durability of this materials combination is found in Fig. 6. Indeed, it shows, for the best performing sample (i.e. 10% wt of CNTs), the different polarization curves and electrochemical parameters from impedance spectroscopy (i.e. ohmic, charge transfer and mass transfer resistances) evaluated after each week of running at constant current, until reaching the 1000 h required to complete the experiments. No sensible variation of performance

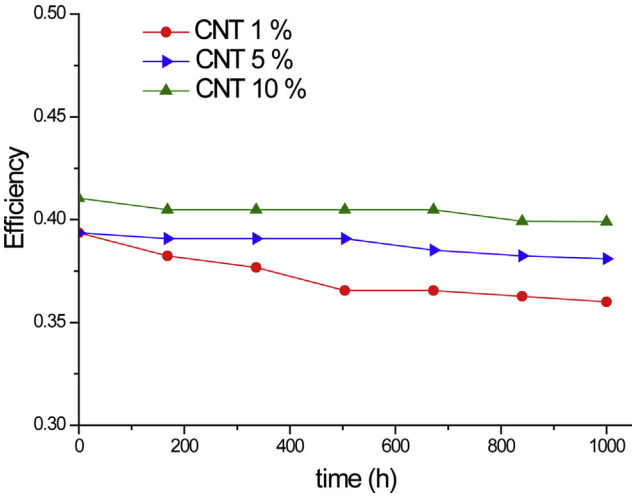


**Fig. 5 – Trends of fuel cell efficiency over time in constant current durability tests for CNTs-based GDMs assembled cells.**

occurred during testing, not only in the ohmic zone, but also in the whole range of current densities, suggesting that also the electrochemical parameters kept constant over the time, as shown by the behavior of the ohmic resistance, the charge transfer resistance and the mass transfer resistance. Ohmic resistance did not show any sensible variation during constant current durability tests, revealing that no evident contribution of GDM to changes in contact resistances or global conductivity occurred. The quasi-constancy of the charge transfer resistance (i.e. the sum of the anodic and the cathodic contribution) along the tests at different times demonstrated that electrodes activity was not affected during these tests. Mass transfer resistance, as expected, increased upon increasing current density because of the diffusive limitations arising from the larger water generation. For this parameter, after 840 h, a small variation between different tests begins to be visible, however it is not enough to cause an appreciable decrease of the global system performance.

### *Accelerated stress tests (ASTs)*

In order to get information on materials response upon prolonged running as well as on the degradation mechanism, chemical and mechanical ASTs were applied (section Accelerated stress tests for experimental details); such tests were performed on the best performing samples, i.e. GDMs with 10% wt of CNTs.

Fig. 7 shows polarization and power density curves obtained on "fresh" (untreated) and chemically degraded GDMs, upon different experiment times (168 h, 336 h, 504 h, 672 h, 840 h, 1000 h). Comparisons between curves were made fixing experiment time. In Fig. 7f, the performance of mechanically degraded GDM upon 1000 h of experiments is also reported, since it was evaluated at the end of the whole AST.

It is evident that after one week of experiments, i.e. 168 h (Fig. 7a), fuel cells assembled with the chemically degraded GDM and the untreated one performed in the same way, being

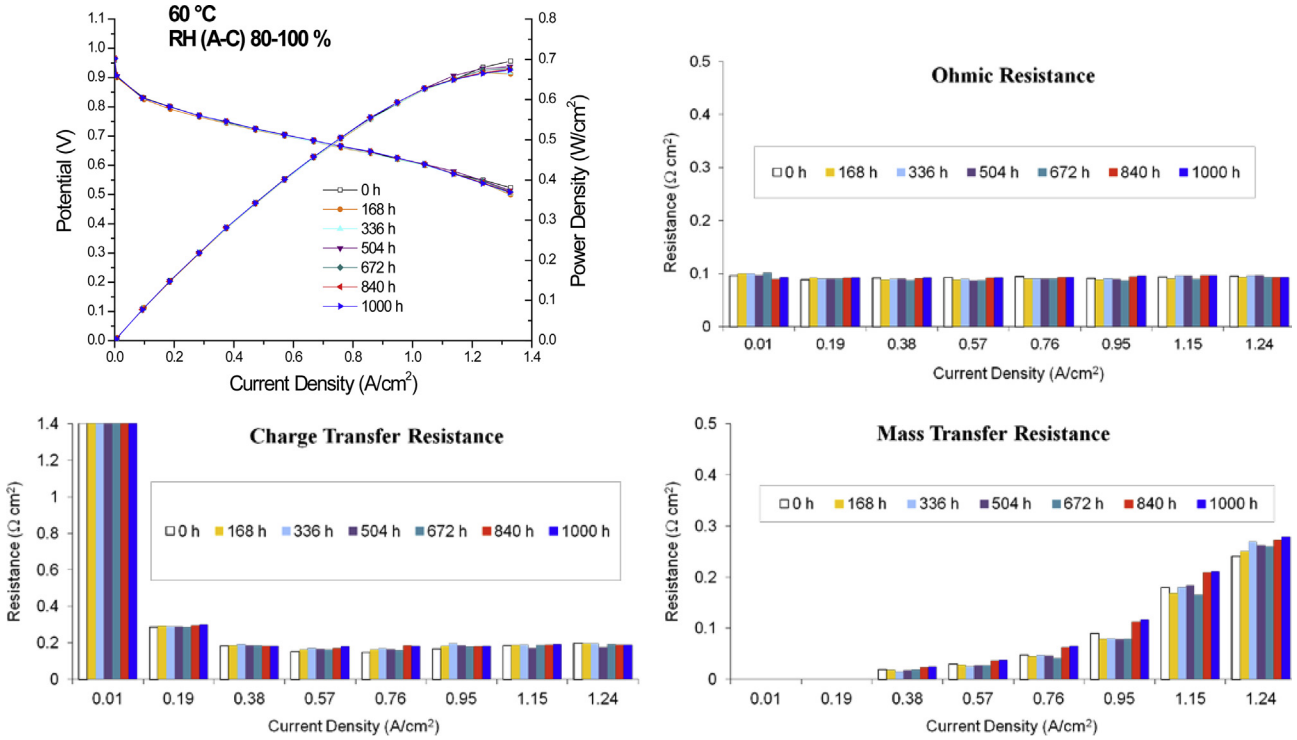


**Fig. 6 – Polarization, power density curves and electrochemical parameters from EIS, obtained at different times of constant current durability tests.**

polarization curves overlapped in the whole range of current density. A slight discrepancy between fresh and stressed GDMs becomes observable upon 336 h of experiments (Fig. 7b) and the gap in performance between them goes on increasing with AST time (c–f). Considering that the most significant differences in the curves occurred in the high current density region, it can be inferred that the GDMs chemical degradation particularly increases the concentration polarization. From Fig. 7f, it is clear that the mechanical AST caused more serious damages in GDM than the chemical one, since polarization and power density curves of the mechanically aged sample showed the worst performance, particularly at high current density; therefore, it can be stated that mechanical degradation plays a more significant role in determining the increase of mass transfer resistances and consequent diffusion limitations.

The fuel cell efficiencies, calculated at significant current density values, namely 0.5, 0.9 and 1.2 A/cm$^2$, are plotted as a function of current density for both chemically and mechanically stressed GDMs and for untreated GDM, upon the whole experiments, i.e. 1000 h (Fig. 8). Being proportional to cell voltage (see section Electrochemical characterization), the efficiency always decreases upon increasing current density. In the ohmic region, i.e. at 0.5 A/cm$^2$, the cell efficiency is almost constant for the three different samples, while it showed sharp changes at 0.9 A/cm$^2$ and even more pronounced at 1.2 A/cm$^2$ (i.e. in the concentration polarization region), in particular after mechanical degradation.

Representative impedance spectra, obtained at low (0.29 A/cm$^2$), medium (0.57 A/cm$^2$) and high (1.15 A/cm$^2$) current density, for the fuel cells assembled with the already discussed GDMs, are reported in Fig. 9. The final target is to evaluate cell performances before and after ASTs and to correlate, if possible, the materials changes to the cell response.

The already discussed equivalent circuit (section Characterization, Fig. 1) has been used for modeling spectra. It is worth noting that the total activation polarization (Rp) is the sum of anodic (Rp,a) and cathodic (Rp,c) contributions.

At any current density, the effects of the stress are evident for high frequency resistances, i.e. the ohmic resistances, as demonstrated by the large differences between fresh and stressed GDMs (Fig. 9). Apart from that, at low current density, arcs with very close diameters were found, suggesting that the charge transfer resistances are not significantly affected by ASTs (Fig. 9a). At medium (Fig. 9b) and especially at high current densities (Fig. 9c), the behavior is different. Indeed, while fresh GDMs revealed a very restrained low frequency arc, i.e. low mass transfer resistance, stressed samples showed very high diffusion resistances. In addition to that, mechanically degraded GDM seems to be the worst sample in water management, since it showed the highest low frequency contribution, which even masks the activation polarization one.

The effects of the stress tests are much more clear when the physical parameters, evaluated on the bases of the EIS, are compared as a function of the current densities. Therefore, in Fig. 10 the ohmic and the mass transfer resistances, i.e. the parameters which are mostly influenced by the GDMs materials features, are plotted for stressed and untreated GDMs, run at constant current, upon different experiment times. It is

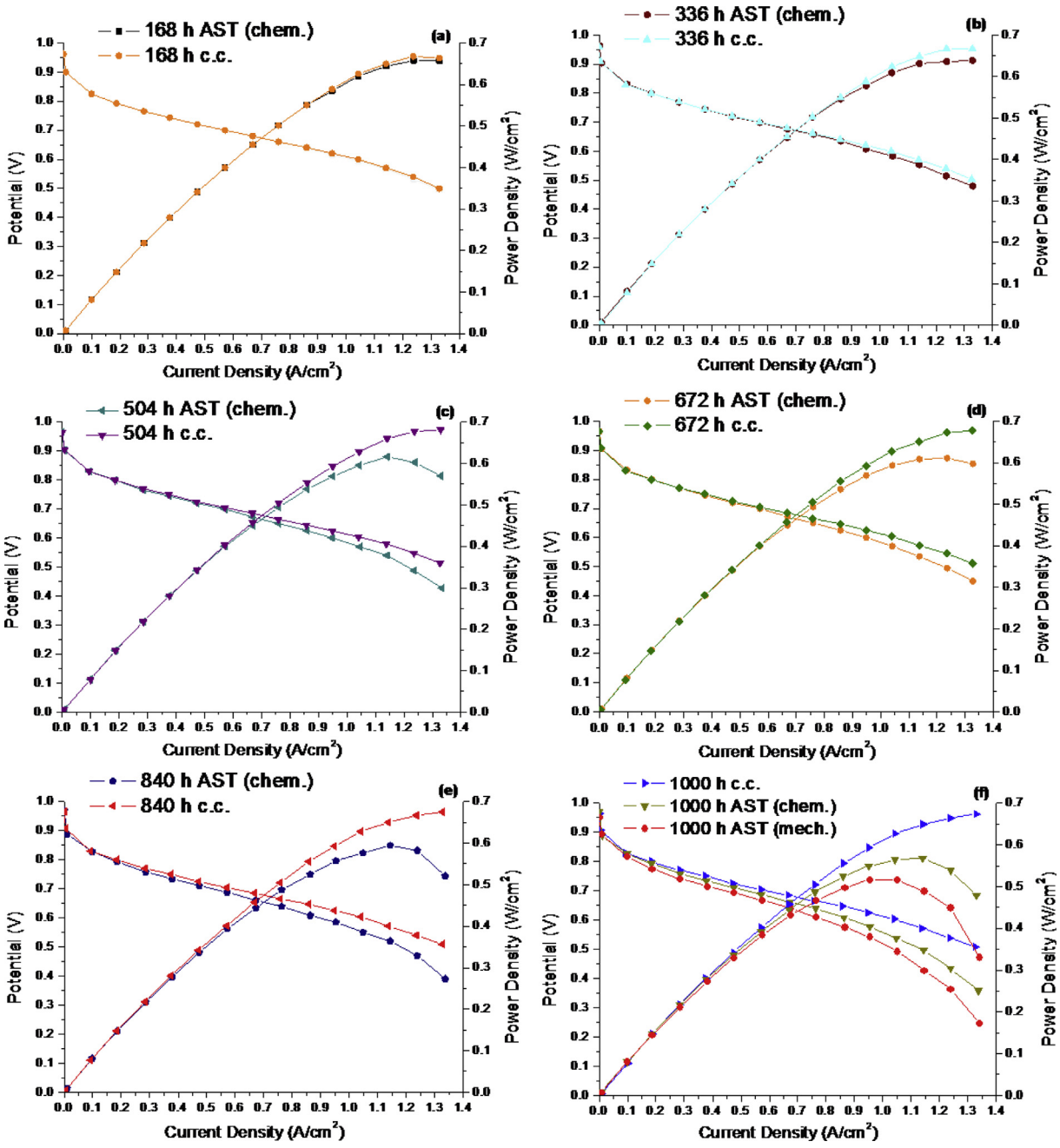


**Fig. 7 – Polarization and power density curves for degraded GDMs and fresh GDMs (subjected at constant current tests, i.e. 'c.c.' in labels) at different treatment times. Performance of the mechanically degraded GDM was evaluated only at the end of the whole experiment, thus only polarization and power density curves upon 1000 h of test are reported for such a GDM.**

worth noting that the resistances related to mechanically degraded samples were obtained only upon 1000 h of experiments (Fig. 10g and h), since performance of such GDMs was evaluated at the end of the whole mechanical AST.

A progressive increase of the ohmic resistance over the time of degradation test was found. The ohmic resistance for chemically degraded GDMs is higher than for fresh GDMs at any time, while a sharp difference in mass transfer resistances is evident starting from 504 h of treatment, particularly at high current density.

From Fig. 10g and h, it is clear that mechanically stressed GDMs, with the highest ohmic resistance, are the worst performing samples. The trend of the mass transfer resistance confirmed that the mechanical degradation induces much more negative effects, on the performance of the running fuel cell, than the chemical one. Indeed, so high resistance values point out a very bad water management after the mechanical ASTs.

All these evidences on electrical performances could be reasonably ascribed to a worsening of physical–chemical

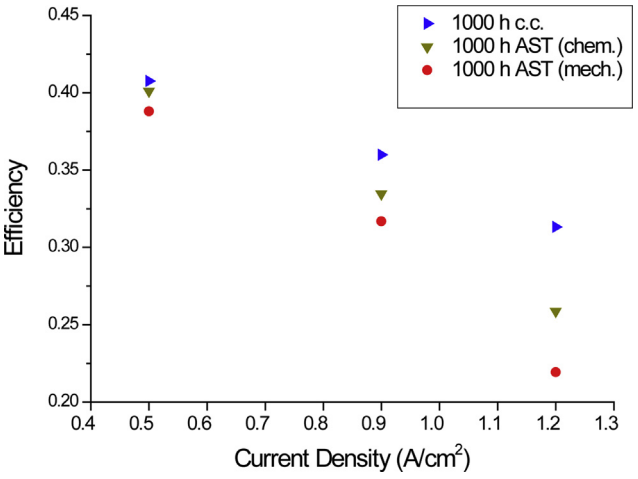


**Fig. 8 – Fuel cell efficiency as a function of current density calculated upon 1000 h of experiments for untreated GDMs, chemically degraded GDMs and mechanically degraded GDMs.**

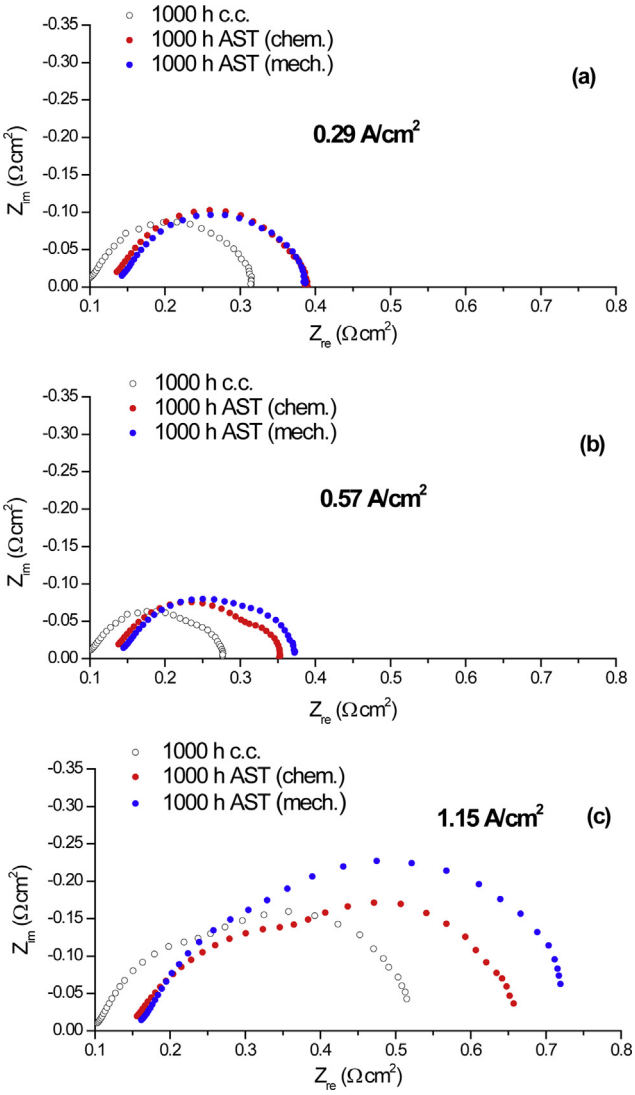


**Fig. 9 – Typical impedance spectra obtained for untreated (run at constant current) and both chemically and mechanically degraded GDMs (after 1000 h) at low (a), medium (b) and high (c) current density.**

properties of the GDMs constituent materials. In order to find a possible correlation degradation-materials properties-performances, SEM images of the GDM CNT 10% (Fig. 11) and static contact angle measurements (Fig. 12) were used in order to determine the effects both of running time and of ASTs on GDMs final quality.

Identifiable cracks, of variable dimensions, are found at the surface of non-stressed sample (Fig. 11a). The presence of cracks is typically related to the thermal treatment process, being due to shrinkage phenomena upon solvent elimination [55]. In principle, cracks formation has to be hampered because it could result in coating detachment during the cell operation. However, if the phenomenon of cracks formation is limited to the layer surface, e.g. less deep cracks are formed, the coating detachment is negligible. Moreover, a positive effect of the presence of slightly deep cracks has been reported: a limited number of cracks may supply alternative paths for species diffusion toward the catalytic region [56]. However, the increase of cracks dimension upon increasing time of ASTs causes severe damages and the observed reduction of performance (Fig. 7).

In Fig. 11f, it can be noticed that the degradation induced by mechanical AST caused more evident damages on the MPL surface: continuous gas flow and compression led to erosion and detachment of large part of the MPL, thus worsening the effectiveness in water removal and increasing the mass transfer resistance. Chemical AST did not deteriorate the MPL as much as mechanical one, even though, after 1000 h of ageing (Fig. 11e), deeper and larger cracks become manifest, being indicative of MPL detachment and of material loss. Anyway, the measured total weight loss of the 1000 h chemically-stressed sample was 3% (w/w) to be compared with that of the mechanically-stressed sample, equal to 20% (w/w). This result is once more a confirmation of the stronger damages on materials in presence of mechanical stress.

These images are also helpful to explain the negative changes of the running cell parameters observed with EIS for samples upon ASTs: material losses and detachment cause surface unevenness, leading to a worse contact between the MPL and the catalyst layer, therefore increasing the overall fuel cell ohmic resistance, particularly in the case of mechanically stressed GDM, the most damaged GDM.

Static contact angle measurements (Fig. 12) pointed out a progressive, but not dramatic decrease of the hydrophobicity for both chemically and mechanically stressed GDMs. Indeed, the values obtained upon degradation experiments (as an example, 147° ± 5° upon 1000 h of chemical AST and 148° ± 5° upon 1000 h of mechanical AST), even lower, are comparable with that of the pristine GDM (158° ± 2°), and in any case still close to the superhydrophobicity range.

This behavior could possibly help to state that hydrophobicity is not the only key parameter to be optimized for water management. If this was the case, no marked effect on mass

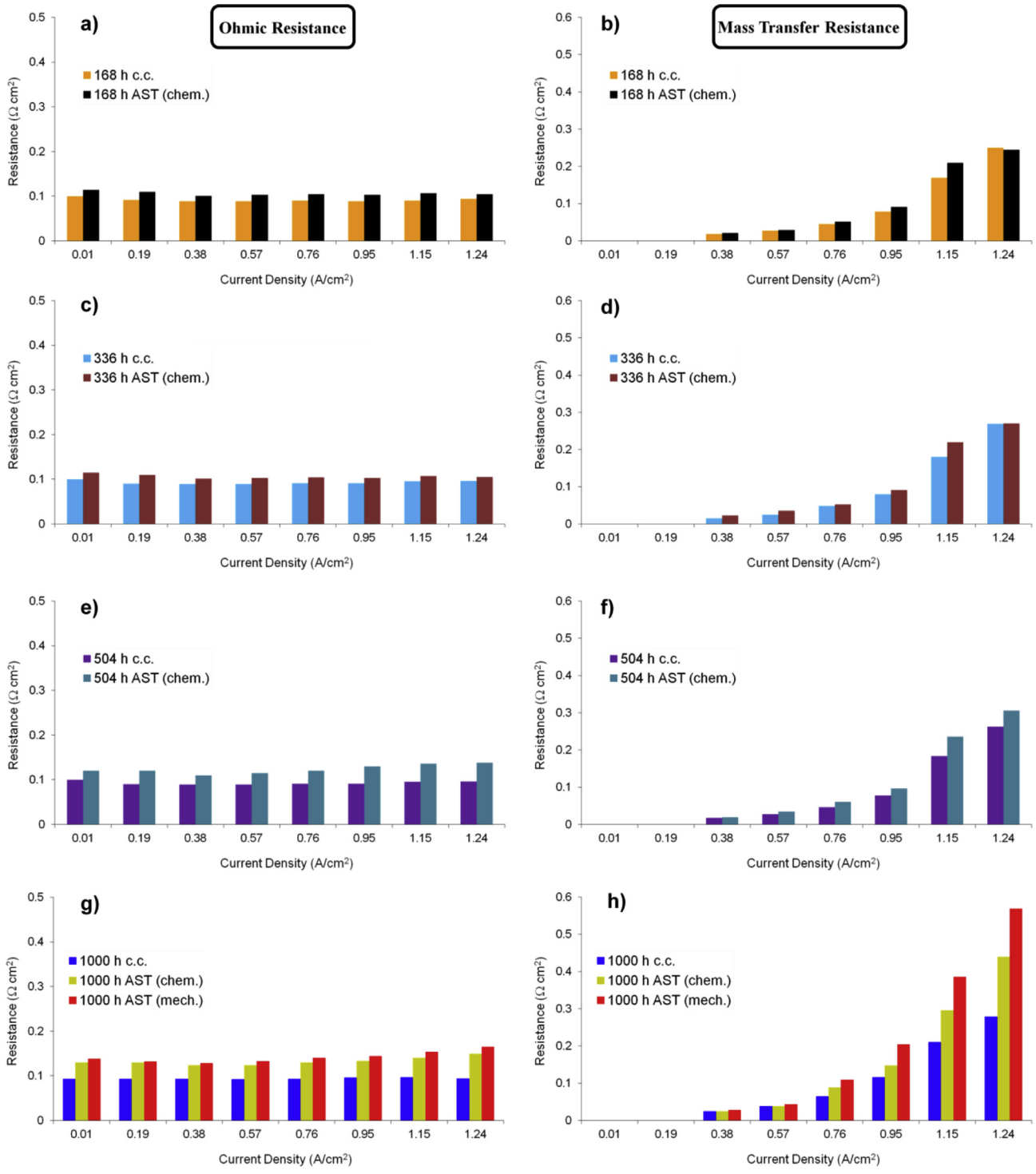


**Fig. 10 – Trend of the ohmic resistance (a, c, e, g) and of the mass transfer resistance (b, d, f, h) as a function of the current density of fuel cells assembled with fresh and degraded GDMs at different times of test. Performance of the mechanically degraded GDM was evaluated only at the end of the whole experiment, thus only resistances upon 1000 h of test are reported for such a GDM.**

transfer resistances had to be detected, even in case of the mechanically stressed GDMs. Thus, the effectiveness in water management seems to be mainly due to the morphology of the surface and to the presence of micro-porosity due to the carbon layer of the MPL.

Such results confirm that ASTs, particularly mechanical AST, strongly influenced surface morphology (see SEM images, Fig. 11) but hydrophobicity was not affected significantly in both cases, contact angle values being close to super-hydrophobic boundary. Thus, the loss in water management

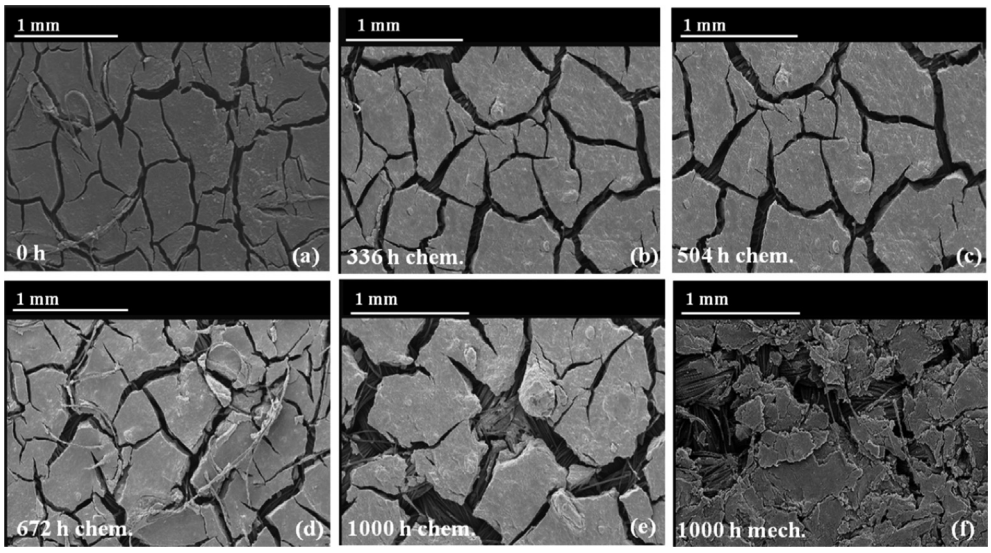


**Fig. 11 – SEM images of fresh GDM (a), chemically degraded (b–e) and mechanically degraded GDM (f).**

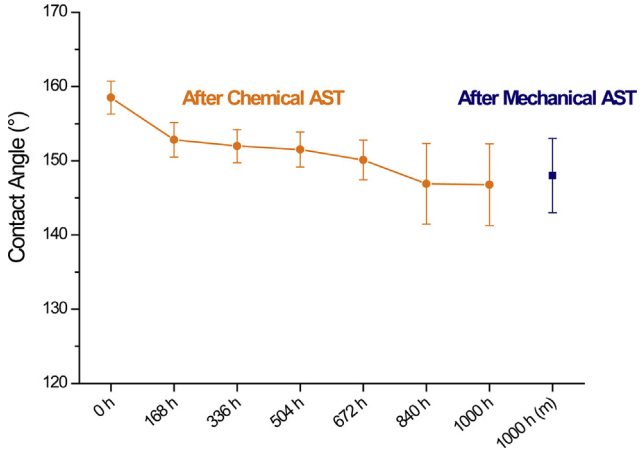


**Fig. 12 – Progression of static contact angle (average value and standard deviation) over time for chemically degraded GDM, compared with the value obtained for mechanically degraded GDM.**

efficiency (i.e. sharp increase in mass transfer resistances observed in Fig. 10) is mainly due to cracks and damages occurring on MPL surfaces and the predominant degradation mechanism seems to be the mechanical one.

## Conclusions

In this work the benefits of FEP, which had been demonstrated to be a better hydrophobic agent than traditionally employed PTFE, and of highly conductive CNTs, have been coupled in the formulation of inks to obtain MPLs. Different CNTs concentrations were adopted.

Shear thinning fluids were obtained and the flow curves were found to be independent on CNTs amount. Rheological behavior and viscosity were suitable for blade coating applications.

The best performance in terms of maximum power density, fuel cell efficiency and durability, upon running the cell for 1000 h of tests, was achieved with the GDM with the highest CNTs content (10% wt).

Ad-hoc chemical and mechanical ASTs on the best performing GDM resulted in a significant increase of both ohmic and mass transfer resistance and in sharp voltage losses mainly in mechanically stressed GDM.

By observing the MPLs surfaces after ASTs, it is clear that the mechanical degradation causes higher damages with respect to the chemical one. However, if a fuel cell operates at medium current densities (i.e. in the ohmic region), durability may be high and efficiency quite constant over long-term tests too.

The increase of mass transfer and ohmic resistances is more likely due to surface damages and loss of material, induced by ASTs, than changes in hydrophobicity. The loss of micro-porous materials brings about an ineffectiveness in water removal.

However, despite of the mass transfer limitations, the fuel cell efficiency calculated in the ohmic region was fairly constant after ASTs, while it suffered a sharp change in concentration polarization region, underlining that flooding phenomena may occur at high current densities in degraded GDMs.

## REFERENCES

[1] Barbir F. PEM fuel cells: theory and practice. 2nd ed. Amsterdam; Boston: Elsevier/Academic Press; 2013.
[2] Park S, Lee JW, Popov BN. A review of gas diffusion layer in PEM fuel cells: materials and designs. Int J Hydrogen Energy 2012;37:5850–65.
[3] Wang Y, Chen KS, Mishler J, Cho SC, Adroher XC. A review of polymer electrolyte membrane fuel cells: technology, applications, and needs on fundamental research. Appl Energy 2011;88:981–1007.

[4] Peighambardoust SJ, Rowshanzamir S, Amjadi M. Review of the proton exchange membranes for fuel cell applications. Int J Hydrogen Energy 2010;35:9349–84.
[5] Yuan XZ, Li H, Zhang SS, Martin J, Wang HJ. A review of polymer electrolyte membrane fuel cell durability test protocols. J Power Sources 2011;196:9107–16.
[6] Chun JH, Jo DH, Kim SG, Park SH, Lee CH, Kim SH. Improvement of the mechanical durability of micro porous layer in a proton exchange membrane fuel cell by elimination of surface cracks. Renew Energy 2012;48:35–41.
[7] Yousfi-Steiner N, Mocoteguy P, Candusso D, Hissel D. A review on polymer electrolyte membrane fuel cell catalyst degradation and starvation issues: causes, consequences and diagnostic for mitigation. J Power Sources 2009;194:130–45.
[8] Wu JF, Yuan XZ, Martin JJ, Wang HJ, Zhang JJ, Shen J, et al. A review of PEM fuel cell durability: degradation mechanisms and mitigation strategies. J Power Sources 2008;184:104–19.
[9] Zhang SS, Yuan XZ, Wang HJ, Merida W, Zhu H, Shen J, et al. A review of accelerated stress tests of MEA durability in PEM fuel cells. Int J Hydrogen Energy 2009;34:388–404.
[10] Panha K, Fowler M, Yuan XZ, Wang HJ. Accelerated durability testing via reactants relative humidity cycling on PEM fuel cells. Appl Energy 2012;93:90–7.
[11] Wu BB, Zhao M, Shi WY, Liu WM, Liu JG, Xing DM, et al. The degradation study of Nafion/PTFE composite membrane in PEM fuel cell under accelerated stress tests. Int J Hydrogen Energy 2014;39:14381–90.
[12] Zhao M, Shi WY, Wu BB, Liu WM, Liu JG, Xing DM, et al. Analysis of carbon-supported platinum through potential cycling and potential-static holding. Int J Hydrogen Energy 2014;39:13725–37.
[13] Park S, Shao YY, Viswanathan VV, Liu J, Wang Y. Non-kinetic losses caused by electrochemical carbon corrosion in PEM fuel cells. Int J Hydrogen Energy 2012;37:8451–8.
[14] Ha T, Cho J, Park J, Min K, Kim HS, Lee E, et al. Experimental study on carbon corrosion of the gas diffusion layer in polymer electrolyte membrane fuel cells. Int J Hydrogen Energy 2011;36:12436–43.
[15] D'Urso C, Oldani C, Baglio V, Merlo L, Arico AS. Towards fuel cell membranes with improved lifetime: aquivion (R) perfluorosulfonic acid membranes containing immobilized radical scavengers. J Power Sources 2014;272:753–8.
[16] DOE. Cell component accelerated stress test protocols for PEM fuel cells, http://www1.eere.energy.gov/hydrogenandfuelcells/. In: DOE, editor.
[17] Rodgers MP, Pearman BP, Mohajeri N, Bonville LJ, Slattery DK. Effect of perfluorosulfonic acid membrane equivalent weight on degradation under accelerated stress conditions. Electrochim Acta 2013;100:180–7.
[18] Kreitmeier S, Schuler GA, Wokaun A, Buchi FN. Investigation of membrane degradation in polymer electrolyte fuel cells using local gas permeation analysis. J Power Sources 2012;212:139–47.
[19] Zhang JL, Song CJ, Zhang JJ. Accelerated lifetime testing for proton exchange membrane fuel cells using extremely high temperature and unusually high load. J Fuel Cell Sci Tech 2011:8.
[20] Park S, Shao YY, Kou R, Viswanathan VV, Towne SA, Rieke PC, et al. Polarization losses under accelerated stress test using multiwalled carbon nanotube supported Pt catalyst in PEM fuel cells. J Electrochem Soc 2011;158:B297–302.
[21] Wu JF, Martin JJ, Orfino FP, Wang HJ, Legzdins C, Yuan XZ, et al. In situ accelerated degradation of gas diffusion layer in proton exchange membrane fuel cell part I: effect of elevated temperature and flow rate. J Power Sources 2010;195:1888–94.
[22] Wu JF, Yuan XZ, Martin JJ, Wang HJ, Yang DJ, Qiao JL, et al. Proton exchange membrane fuel cell degradation under close to open-circuit conditions part I: in situ diagnosis. J Power Sources 2010;195:1171–6.
[23] Shao YY, Wang J, Kou R, Engelhard M, Liu J, Wang Y, et al. The corrosion of PEM fuel cell catalyst supports and its implications for developing durable catalysts. Electrochim Acta 2009;54:3109–14.
[24] Borup R, Meyers J, Pivovar B, Kim YS, Mukundan R, Garland N, et al. Scientific aspects of polymer electrolyte fuel cell durability and degradation. Chem Rev 2007;107:3904–51.
[25] Bae SJ, Kim SJ, Park JI, Lee JH, Cho H, Park JY. Lifetime prediction through accelerated degradation testing of membrane electrode assemblies in direct methanol fuel cells. Int J Hydrogen Energy 2010;35:9166–76.
[26] Cho J, Ha T, Park J, Kim HS, Min K, Lee E, et al. Analysis of transient response of a unit proton-exchange membrane fuel cell with a degraded gas diffusion layer. Int J Hydrogen Energy 2011;36:6090–8.
[27] Yu SC, Li XJ, Liu S, Hao JK, Shao ZG, Yi BL. Study on hydrophobicity loss of the gas diffusion layer in PEMFCs by electrochemical oxidation. Rsc Adv 2014;4:3852–6.
[28] Spernjak D, Fairweather J, Mukundan R, Rockward T, Borup RL. Influence of the microporous layer on carbon corrosion in the catalyst layer of a polymer electrolyte membrane fuel cell. J Power Sources 2012;214:386–98.
[29] Lee C, Merida W. Gas diffusion layer durability under steady-state and freezing conditions. J Power Sources 2007;164:141–53.
[30] Schulze M, Wagner N, Kaz T, Friedrich KA. Combined electrochemical and surface analysis investigation of degradation processes in polymer electrolyte membrane fuel cells. Electrochim Acta 2007;52:2328–36.
[31] Kim T, Lee S, Park H. A study of water transport as a function of the micro-porous layer arrangement in PEMFCs. Int J Hydrogen Energy 2010;35:8631–43.
[32] Kitahara T, Konomi T, Nakajima H. Microporous layer coated gas diffusion layers for enhanced performance of polymer electrolyte fuel cells. J Power Sources 2010;195:2202–11.
[33] Wang YX, Al Shakhshir S, Li XG. Development and impact of sandwich wettability structure for gas distribution media on PEM fuel cell performance. Appl Energy 2011;88:2168–75.
[34] Kandlikar SG, Garofalo ML, Lu Z. Water management in a PEMFC: water transport mechanism and material degradation in gas diffusion layers. Fuel Cells 2011;11:814–23.
[35] Ha T, Cho J, Park J, Min K, Kim HS, Lee E, et al. Experimental study of the effect of dissolution on the gas diffusion layer in polymer electrolyte membrane fuel cells. Int J Hydrogen Energy 2011;36:12427–35.
[36] Pasaogullari U, Wang CY. Two-phase transport and the role of micro-porous layer in polymer electrolyte fuel cells. Electrochim Acta 2004;49:4359–69.
[37] Weber AZ, Newman J. Effects of microporous layers in polymer electrolyte fuel cells. J Electrochem Soc 2005;152:A677–88.
[38] Kim S, Ahn BK, Mench MM. Physical degradation of membrane electrode assemblies undergoing freeze/thaw cycling: diffusion media effects. J Power Sources 2008;179:140–6.
[39] Oszcipok M, Riemann D, Kronenwett U, Kreideweis M, Zedda A. Statistic analysis of operational influences on the cold start behaviour of PEM fuel cells. J Power Sources 2005;145:407–15.
[40] Frisk J, Boand W, Kurkowski M, Atanasoski R, Schmoeckel A. In: Fuel cell seminar, San Antonio, TX, USA; 2004.
[41] Wood D, Davey J, Garzon F, Atanassov P, Borup RL. In: Fuel cell seminar, Palm Springs, CA; 2005.

[42] Latorrata S, Stampino PG, Cristiani C, Dotelli G. Novel superhydrophobic microporous layers for enhanced performance and efficient water management in PEM fuel cells. Int J Hydrogen Energy 2014;39:5350–7.
[43] Lim C, Wang CY. Effects of hydrophobic polymer content in GDL on power performance of a PEM fuel cell. Electrochim Acta 2004;49:4149–56.
[44] Borup RL, Davey JR, Garzon FH, Wood DL, Inbody MA. PEM fuel cell electrocatalyst durability measurements. J Power Sources 2006;163:76–81.
[45] Song JM, Uchida H, Watanabe M. Effect of wet-proofing treatment of carbon backing layer in gas diffusion electrodes on the PEFC performance. Electrochemistry 2005;73:189–93.
[46] Yan WM, Hsueh CY, Soong CY, Chen FL, Cheng CH, Mei SC. Effects of fabrication processes and material parameters of GDL on cell performance of PEM fuel cell. Int J Hydrogen Energy 2007;32:4452–8.
[47] Park SB, Park YI. Fabrication of gas diffusion layer (GDL) containing microporous layer using flourinated ethylene prophylene (FEP) for proton exchange membrane fuel cell (PEMFC). Int J Precis Eng Man 2012;13:1145–51.
[48] Purwanto WW, Slamet, Wargadalam VJ, Pranoto B. Effects of the addition of flourinated polymers and carbon nanotubes in microporous layer on the improvement of performance of a proton exchange membrane fuel cell. Int J Electrochem Sci 2012;7:525–33.
[49] Hung CJ, Liu CH, Ko TH, Chen WH, Cheng SH, Chen WS, et al. Effect of diffusion layers fabricated with different fiber diameters on the performance of low temperature proton exchange membrane fuel cells. J Power Sources 2013;221:134–40.
[50] Stampino PG, Omati L, Cristiani C, Dotelli G. Characterisation of nanocarbon-based gas diffusion media by electrochemical impedance spectroscopy. Fuel Cells 2010;10:270–7.
[51] Latorrata S, Stampino PG, Amici E, Pelosato R, Cristiani C, Dotelli G. Effect of rheology controller agent addition to micro-porous layers on PEMFC performances. Solid State Ionics 2012;216:73–7.
[52] Yuan XZ, Song C, Wang H, Zhang J. Electrochemical impedance spectroscopy in PEM fuel cells. Fundamentals and applications. New York: Springer; 2010. p. 1–420.
[53] Ramasamy RP, Kumbur EC, Mench MM, Liu W, Moore D, Murthy M. Investigation of macro- and micro-porous layer interaction in polymer electrolyte fuel cells. Int J Hydrogen Energy 2008;33:3351–67.
[54] Tracton AA. Coatings technology handbook. 3rd ed. Boca raton, FL: Taylor & Francis; 2005.
[55] Kong CS, Kim DY, Lee HK, Shul YG, Lee TH. Influence of pore-size distribution of diffusion layer on mass-transport problems of proton exchange membrane fuel cells. J Power Sources 2002;108:185–91.
[56] Lee HK, Park JH, Kim DY, Lee TH. A study on the characteristics of the diffusion layer thickness and porosity of the PEMFC. J Power Sources 2004;131:200–6.